Supplementary Information

A Scalable Optofluidic Microreactor with Immobilized Pt-CdS Catalysts for Visible Light-Driven Photocatalytic Hydrogen Evolution from Water

*Ameer Suhail [a], D Pamu [a,b], Nageswara Rao Peela [a,c,]**

[a] Centre for Nanotechnology, Indian Institute of Technology Guwahati, Guwahati, 781039, Assam, India

[b] Department of Physics, Indian Institute of Technology Guwahati, Guwahati, 781039, Assam, India

[c] Department of Chemical Engineering, Indian Institute of Technology Guwahati, Guwahati, 781039, Assam, India

* Corresponding author: Nageswara Rao Peela, E-mail: peelanr@iitg.ac.in, Phone: + 91-361-2583526

Note S1. Materials

Commercial window glass sheets (152 mm × 102 mm × 3 mm) were purchased from Saint Gobain Glass, India. The two-component epoxy paint mixture with thinner was purchased from Taralac, India. Hydrofluoric acid (HF, 40%) was purchased from Finar Chemicals, India. Cadmium nitrate ($Cd(NO_3)_2 \cdot 4H_2O$), Thiourea (CH_4N_2S), Ethylenediamine ($C_2H_8N_2$), and Potassium hexachloroplatinate (K_2PtCl_6) were purchased from Sigma Aldrich, USA. 3-Aminopropyltriethoxysilane (APTES) was purchased from Himedia, India. Colloidal silica (SiO_2, 12 nm, Ludox HSA) was purchased from Grace Inc., USA. Polytetrafluoroethylene (PTFE) tubing was purchased from Cole-Parmer, India. Epoxy adhesive glue (Rapid and Clear Adhesive) was purchased from Fevitite, India. UV glue was purchased from Excel Impex, India. Glass drill bits, 5 mm thick PMMA sheet pieces (25 mm × 25 mm), and pressing clips were locally purchased. All the chemicals involved were of analytical grade and were used as received without further purification. DI water for different processes was taken from an in-house millipore unit (Model: Elix-3, Make: Millipore, The USA).

Note S2. Safety Protocols for Hydrofluoric Acid (HF) Etching

The wet chemical etching process utilizes concentrated Hydrofluoric Acid (HF, 40%), which poses severe health risks upon contact or inhalation. To ensure reproducibility and personnel safety, the following strict protocols were adhered to during all fabrication steps:

- Engineering Controls: All etching operations were conducted exclusively inside a certified chemical fume hood with active exhaust ventilation to prevent inhalation of HF vapors.
- Personal Protective Equipment (PPE): Operators were equipped with a full-face shield, heavy-duty butyl rubber gloves (specifically rated for HF resistance), and a chemical-resistant apron worn over a standard laboratory coat.

- Emergency Response: A tube of Calcium Gluconate gel (2.5%) was maintained immediately accessible at the workstation as a first-response antidote for potential skin exposure.
- Waste Disposal: Post-etching, the spent HF solution was neutralized with excess calcium carbonate ($CaCO_3$) to precipitate fluoride ions as insoluble calcium fluoride (CaF_2) prior to disposal in accordance with hazardous waste regulations.

Note S3. Characterization Instruments and Parameters

Reactor Plate: The fabricated samples at different stages of the process were subjected to different characterizations such as basic wide-angle magnified photography (Model: 12MP Wide camera, iPad Air 4; Make: Apple Inc., USA), optical microscopy (Model: AXIO Scope A1; Make: Carl Zeiss NTS Ltd), scanning electron microscopy (Model: JSM-7610F, Make: JEOL Japan), and contact profilometry (Model: Dektak 150, Make: Veeco Instruments Inc.). While top view scanning electron microscopy and optical microscopy was used to examine the features, edges, dimensions, and surface texture of the fabricated samples, cross-sectional SEM analysis was done to determine the height/depth of the chambers and microstructures. Profilometry was employed to assess the surface topology, height profile, and surface roughness of the microchannels. The wide-angle magnified photography enabled the imaging of the full sized microreactor plates at different stages of the fabrication process. These characterization techniques provided valuable insights into the quality and effectiveness of the microchannel fabrication process, guiding the optimization and refinement as needed.

Photocatalyst Powder: The as-synthesized and Pt-modified CdS nanowires were characterized using various techniques to evaluate their properties. Scanning Electron Microscopy (Model: JSM-7610F, Make: JEOL, Japan) was employed to assess the nanowires' morphology (length, diameter, and aspect ratio). X-ray Diffraction (Model: SmartLab, Make: Rigaku, Japan) provided a preliminary investigation of the samples' crystal structure and phase composition. UV-Visible Spectroscopy (Model: UV-2600, Make: Shimadzu, Japan) was utilized to determine the bandgap of the CdS nanowires by analyzing their absorbance spectra. X-ray Photoelectron Spectroscopy (Model: PHI 5000 VERSAPROBE III, Make: ULVAC-PHI, Inc., Japan) allowed for the analysis of surface composition, oxidation states, and valence band spectra of the nanowires. High-resolution images of the nanowires, including lattice fringes with the corresponding d-spacing and electron diffraction patterns, were obtained using Transmission Electron Microscopy (Model: JEM-2100F, Make: JEOL,Japan). Lastly, Energy-dispersive X-ray Spectroscopy (Model: Sigma, Make: Zeiss, Germany) was employed to evaluate the elemental composition and contrast within the samples.

Photocatalyst Coating: The photocatalyst coatings were characterized after the coating process for optimization and validation. Scanning Electron Microscopy (Model: JSM-7610F, Make: JEOL, Japan) was utilized to examine the coated catalyst layer's morphology, thickness, and uniformity, while Energy-Dispersive X-ray Spectroscopy (Model: Sigma, Make: Zeiss, Germany) provided insight into the elemental composition and distribution within the layer. Thin film X-ray Diffraction (Model: SmartLab, Make: Rigaku, Japan) provided details of the coatings' crystal structure and phase composition. Additionally, Atomic Force Microscopy

(AFM, Model: Innova, Make: Bruker, USA) was employed to measure the surface profile and thickness of the catalyst coating.

Note S4. Particle Suspension Reactor Setup

The experimental setup for particle suspension reactor comprised a light-tight enclosure to prevent the entry of stray light. Housed within this chamber was a 250 W LED lamp (Model: Challenger Pro-CFS-506-250-57-10D-HL3-GL-NBR, Make: Crompton, India) positioned at a distance of 13 cm from a 500 mL quartz volumetric flask containing the reaction mixture. A magnetic stirrer was incorporated to facilitate continuous stirring of the reaction mixture. The reaction vessel was supplied with N_2 gas from a N_2 cylinder, and its outlet was connected to an in-line Gas Chromatography (Model: 7890A, Make: Agilent, USA) equipped with a CP-molecular sieves 5A column and a thermal conductivity detector (TCD). The continuous stream of N_2 transported the generated H_2 gas from the reaction vessel into the Gas Chromatography Analyzer. Before the reaction, the reaction mixture was prepared by dissolving 0.1 M Na_2S/Na_2SO_3 (sacrificial reagent) in 400 mL of deionized water, followed by the addition of 50 mg of Pt-loaded CdS nanowire photocatalyst (125 mg/L). This mixture was sonicated for 15 min to ensure proper dispersion. After connecting the reaction vessel with the inlet and outlet lines of the setup, while keeping the lamp in the OFF state, a continuous flow of N_2 gas at 30 mL/min for 30 min was supplied to purge the reaction vessel to remove the oxygen gas present inside the chamber. After purging, the photocatalytic reaction was initiated by turning on the LED lamp. A N_2 flow rate of 5 mL/min and a GC sampling interval of 10 min were used while carrying out the photocatalytic reaction.

Note S5. Quantum Efficiency for Photocatalytic Hydrogen Evolution

1. Power Density and Incident Radiation

The quantum efficiency (QE) of the photocatalytic hydrogen evolution reaction (HER) was evaluated through a detailed photophysical analysis. The LED lamp power measurements were conducted using a detector with a 12 mm diameter.

Detector area calculation: $A_{detector} = \pi(\text{diameter}/2)^2 = \pi(0.012\ \text{m}/2)^2 \approx 1.13 \times 10^{-4}\ \text{m}^2$

Power density determination: $P_{density} = P_{detector} / A_{detector} = 0.15\ \text{W} / (1.13 \times 10^{-4}\ \text{m}^2) \approx 1327.43\ \text{W/m}^2$

Reactor illumination area was determined from geometric dimensions: $A_{reactor} = (3 \times 0.0254\ \text{m}) \times (2.5 \times 0.0254\ \text{m}) = 4.84 \times 10^{-3}\ \text{m}^2$

Total power incident on reactor: $P_{reactor} = P_{density} \times A_{reactor} = 1327.43\ \text{W/m}^2 \times 4.84 \times 10^{-3}\ \text{m}^2 \approx 6.43\ \text{W}$

2. Photon Energy for 5700 K LED Spectrum

Photon energy calculation based on wavelength: $E_{photon} = hc/\lambda$

Where:

- $h = 6.626 \times 10^{-34}$ J·s (Planck's constant)
- $c = 3.0 \times 10^8$ m/s (speed of light)
- λ = wavelength in meters

Photon energy range (400–700 nm):

- λ = 400 nm: E_{photon} = 3.10 eV

- $\lambda = 700$ nm: Ephoton = 1.77 eV

Average photon energy calculation: Ephoton = $[\int(hc/\lambda \cdot I(\lambda)\, d\lambda)] / [\int I(\lambda)\, d\lambda]$
Where $I(\lambda)$ represents spectral intensity distribution according to Planck's radiation law: $I(\lambda) = [2hc^2/\lambda^5] \cdot [1 / (\exp(hc/\lambda kBT) - 1)]$
Parameters:

- kB = 1.381×10^{-23} J/K (Boltzmann constant)
- T = 5700 K (LED color temperature)

Simplified average photon energy: 2.24 eV (This value represents a numerically integrated approximation of the photon energy distribution for the 5700 K LED spectrum, accounting for the non-uniform spectral intensity across the visible range.)

3. Photon Flux and Hydrogen Production

Photon energy calculation: Ephoton = 2.24 eV = $2.24 \times 1.602 \times 10^{-19}$ J ≈ 3.59×10^{-19} J
Photon flux calculation: Φphotons = Preactor / Ephoton = 6.43 W / (3.59×10^{-19} J) ≈ 1.79×10^{19} photons/second
Hydrogen production rate conversion: H_2 molecules/second = (60.7×10^{-6} mol/hour / 3600 s/hour) × 6.022×10^{23} molecules/mol ≈ 1.02×10^{16} molecules/second
Photons used for hydrogen production: Photons used = $2 \times 1.02 \times 10^{16} \approx 2.04 \times 10^{16}$ photons/second

4. Quantum Efficiency

Quantum efficiency determination: QE = (Photons used / Incident photons) × 100 = ($2.04 \times 10^{16} / 1.79 \times 10^{19}$) × 100 ≈ 0.11%

Note S6. Detailed Economic Analysis and Scalability Calculations

A. Detailed Cost Breakdown
A comprehensive itemization of all material and equipment costs associated with fabricating the 48.6 cm^2 reactor is provided below.
Table S1. Detailed cost breakdown for fabrication of the 48.6 cm^2 optofluidic microreactor.

Cost Category	Item	Specification	Unit Cost (INR)	Unit Cost (USD)	Quantity / Usage	Cost per Reactor (INR)	Cost per Reactor (USD)	Notes
Substrate	Fused silica window glass	3 mm thickness	₹500/m^2	\$5.56/m^2	0.03 m^2 (2 plates)	**₹15.00**	**\$0.17**	Commercial grade
Etch Mask	Epoxy paint	Industrial grade	₹600/L	\$6.67/L	20 mL	**₹12.00**	**\$0.13**	Reusable for multiple reactors
Etching	HF acid (40%)	Scientific grade	₹1,200/L	\$13.33/L	15 mL	**₹18.00**	**\$0.20**	Optimized volume
Catalyst	CdS synthesis batch	$Cd(NO_3)_2$, Thiourea, Ethylenediamine	₹500/batch	\$5.56/batch	~6.7% of batch	**₹33.50**	**\$0.37**	For 50 mg loading

	Pt precursor	K_2PtCl_6	₹14,000/g	$155.55/g	0.13 mg	**₹2.00**	**$0.02**	For 0.1 wt% Pt loading
	Coating Primer	APTES	₹4,500/100g	$50.00/100g	~0.1 g	**₹4.50**	**$0.05**	Adhesion promoter
	Colloidal silica binder	Ludox HSA	₹4,500/L	$50.00/L	1 mL	**₹4.50**	**$0.05**	Binder ratio 1:1
Sealing	Top glass plate	(Included in Substrate)	-	-	-	-	-	Accounted for above
	UV-curable adhesive	Excel Impex	₹350/unit	$3.89/unit	1 mL	**₹15.00**	**$0.17**	
	Epoxy adhesive	Fevitite	₹55/pack	$0.61/pack	1 g	**₹4.00**	**$0.04**	
Fluidics	Rigid PTFE tubing	Industrial Grade 1/16"	₹150/m	$1.67/m	0.6 m	**₹90.00**	**$1.00**	Standard industrial spool rate
	Acrylic stabilizers	Laser-cut sheet	₹450/sq.ft	$5.00/sq.ft	2 pieces	**₹10.00**	**$0.11**	
Equipment	Paint gun	Buildskill Pro	₹5,000	$55.55	Amortized (1000x)	**₹5.00**	**$0.06**	One-time investment
(Amortized)	Laser engraver	Ortur Laser Master 2	₹30,000	$333.33	Amortized (1000x)	**₹30.00**	**$0.33**	One-time investment
	Airbrush	Iwata commercial	₹20,000	$222.22	Amortized (1000x)	**₹20.00**	**$0.22**	One-time investment
Energy	Electricity	Laser + Curing (UV + Thermal)	₹8/kWh	$0.09/kWh	5 kWh	**₹40.00**	**$0.44**	For 4.5h laser operation
TOTAL						**₹303.50**	**$3.37**	**Total per reactor**

Note: Exchange rate used: 1 USD ≈ ₹90.

B. Cost Projection for Scaled Systems

Based on the cost breakdown, we calculated the projected cost per unit area for reactors of different scales.

Table S2. Projected cost per m^2 for optofluidic microreactors of different scales.

Reactor Scale	**Specification**	**Basis of Calculation**	**Material Cost (INR)**	**Equipment Cost (INR)**	**Total Cost (INR)**	**Total Cost (USD)**	**Normalized Cost (per m2)**
Lab Prototype	**Area:** 48.6 cm^2 (0.00486 m^2) **Unit:** 1 Chip	**Direct Costing:** derived from Table S1. • *Energy:* 5 kWh • *Equipment:*	₹248.50	₹55.00	**₹303.50**	**$3.37**	**$694/m²**

		Amortized base rate.					
Large-Area Plate	**Area:** 579.1 cm^2 (0.058 m^2) **Unit:** 1 Plate	**Linear Scaling:** Area increases by **11.9x**. • *Consumables :* Scaled 11.9x. • *Energy & Equipment:* Scaled 11.9x • *Fluidics:* Fixed estimate (₹200).	₹1,967.00	₹655.00	**₹2,622.00**	**$29.13**	**$503/m²**
Scaled System	**Area:** 1.45 m^2 **Unit:** 25 Modules	**5 × 5 Modular Array:** • *Calculation:* 25 × Plate Cost. • *Note:* 10% bulk discount applied to materials only.	₹44,250.00	₹16,375.00	**₹60,625.00**	**$673.61**	**$465/m²**

Note: Exchange rate used: 1 USD = ₹90.

C. Comparative Analysis against Photolithography

To contextualize the advantages of our fabrication approach, we provide a direct comparison with conventional photolithography-based microfabrication in terms of both economic cost (Table S3) and technical scalability (Table S4).

Table S3. Economic cost comparison between laser lithography and photolithography methods.

Cost Component	**Photolithography Method**	**Laser Lithography Method (This Work)**	**Cost Ratio**
Equipment			
Primary tool	Mask aligner: ₹10–50 lakhs ($11,000–55,000)	Laser engraver: **₹30,000** ($333)	**~30–160× lower**
Coating tool	Spin coater: ₹2–10 lakhs ($2,200–11,000)	Paint spray gun: **₹5,000** ($56)	**~40–200× lower**
Total Capital Investment	**₹12–60 lakhs ($13,200–66,000)**	**₹35,000 ($389)**	**~35–170× lower**
Consumables			
Resist/mask material	SU-8 photoresist: ~₹3,56,500/L ($3,961/L)	Epoxy paint: **₹600/L** ($6.67/L)	**~594× lower**
Developer	SU-8 Developer: ~₹49,000/L	**Not required** (laser	**Infinite saving**

	($544/L)	ablation)	
Infrastructure			
Cleanroom requirement	**Yellow room (UV-free)** with controlled humidity/dust	**Standard laboratory bench**	**Significant cost saving**

Table S4. Technical scalability comparison between laser lithography and photolithography methods.

Aspect	**Photolithography**	**Laser Lithography (This Work)**
Maximum substrate size	~100 mm × 100 mm (limited by standard photomasks, spin coaters, mask writers, and mask aligners)	**400 mm × 400 mm** (current system); upgradeable to larger
Pattern transfer method	Multi-step: coating, baking, exposure, development	**Single-step:** direct laser ablation
Resist mechanical strength	SU-8 often delaminates during deep HF etching (>100 μm)	**Epoxy mask** highly robust for deep glass etching (>200 μm)
Cleanroom requirement	Yes (UV-free environment)	**No**
Fabrication time per reactor	15–20 hours (multi-step process including coating, baking, exposure, and development)	**~4.5 hours** (single-step automated patterning)
Scalability to 1 m²	Not technically feasible with standard configuration	**Feasible** via modular tiling of large plates

D. Literature Comparison

Table S5. Comparison of reactor fabrication costs with literature-reported photocatalytic systems.

Reactor Type	**Reference**	**Reactor Scale**	**Reported Cost**	**Normalized Cost (per m²)**	**Notes**
Suspension Pilot Plant	1,2	Pilot Scale (CPC Array)	High CapEx & OpEx	~$300 – $600 / m²	Glass tube array with CPC reflectors; suffers from catalyst settling and high gas separation costs.
Immobilized Panel Reactor	3,4	Large Scale (1 m² – 100 m²)	~$150 per module	~$100 – $160 / m²	Screen-printed flat panels; scalable but suffers from mass transfer limitations (stagnant water layers).
Microfluidic Reactor	5,6	Chip Scale (<50 cm²)	>$100 per chip	>$10,000 / m²	Precision milling/bonding; high durability/surface area but prohibitively expensive for large-scale energy applications.
This work (OFMR)	This Work	1.45 m² (scaled)	$673.61 (system)	~$465 / m²	Laser lithography method; combines microfluidic efficiency with scalable cost and no catalyst separation.

Note S7. Performance Benchmarking and Contextual Analysis

Table S6. Comprehensive performance benchmarking of the micro-patterned Optofluidic Microreactor (OFMR) developed in this work against state-of-the-art photocatalytic systems reported in the literature. The systems are categorized by reactor configuration: (i) Microfluidic Reactors, (ii) Scalable Rigid/Fixed Panel Reactors, and (iii) Scalable Flexible Membrane Panel Reactors. Performance is compared using area-normalized hydrogen evolution rates (R_{area}), mass-normalized rates (R_{mass}), and efficiency metrics such as Solar-to-Hydrogen (STH) efficiency or Apparent Quantum Yield (AQY).

System Category	Ref	Reactor Configuration	Photocatalyst	Light Source	H_2 Rate (Area) (mmol m^{-2} h^{-1})	H_2 Rate (Mass) (mmol g^{-1} h^{-1})	Efficiency (STH / AQY)	Key Features & Scalability
This Work	-	Optofluidic Microreactor (Micro-patterned)	Pt-CdS	LED (Visible)	12.48	1.21	AQY: 0.11%	Scalable laser-patterning; Continuous flow; Active bubble removal.
Microfluidic Reactors	[7]	Corrugated Serpentine OFMR (Glass)	CdS/g-C_3N_4 (In-situ nanowires)	Vis. (Metal Halide)	~60.7	-	AQY: 29.6% (P-SOFMR)	Chaotic advection mixing; 3D microstructure; Flow rate 1.0 mL/min.
	[8]	Serpentine OFMR (Glass)	CdS (Sol-gel coating)	Vis. (Metal Halide)	26.5	-	-	Adhesive tape fabrication; High surface-to-volume ratio.
	[6]	Micro-pillared Optofluidic (PDMS/Si)	Pt/TiO_2	UV (Hg Lamp)	*Not Reported*	-	-	56% rate enhancement vs. planar; Pillars induce flow

								perturbation.
	[5]	Micro-grooved Optofluidic (PDMS)	Pt/TiO_2	UV (Hg Lamp)	*Not Reported*	-	-	Casting-transfer fabrication; Higher durability than spray coating.
Scalable Panel Reactors (Rigid/Fixed)	[9]	Concentrated Panel (4×4 cm^2)	InGaN/GaN Nanowires	Natural Sunlight (Concentrated ~160x)	~160,000	-	STH: 6.2% (Outdoor) STH: 9.2% (Indoor)	Highest Rate; High-intensity operation (16,070 mW cm^{-2}); Temp. optimized (70°C).
	[4]	100 m^2 Panel Array	$SrTiO_3$:Al (Rh/Cr_2O_3/CoOOH)	Natural Sunlight	~103	-	STH: 0.76% (Max)	Largest Scale (1600 units); Gas separation membrane; Safe H_2/O_2 handling.
	[3]	1 m^2 Flat Panel	$SrTiO_3$:Al (Sheet)	Natural Sunlight	~28	-	STH: 0.4%	1 mm water layer; Rapid bubble release; Hydrophilic window.
	[10]	Metal Plate Reactor (0.76 m^2)	Carbon Nitride (Pt@mp-CN)	Natural Sunlight	~33	-	STH: 0.12%	Immobilized on stainless steel; Drop-coating with Nafion binder.
Scalable Panel	[11]	Membrane Panel	CdS@SiO_2-Pt	Sim. Sunlight	213.48	6.24	STH: 0.68%	State-of-the-Art

Reactors (Flexible Membrane)		(16×23 cm^2)	/ PVDF	(Xe Lamp)			(Membrane) STH: 0.05% (Panel)	Membrane Rate; 50-cycle stability; Alkaline (pH 14).
	[12]	Membrane Panel	Sb_2S_3-NiS / PVDF	Sim. Sunlight + Ultrasound	15.71	3.45	STH: 0.06%	Piezo-photocatalytic (40 Hz); 280 h durability; Alkaline (pH 13).
	[13]	Membrane Panel	MoS_2/TiO_2-Pt / PVDF	Sim. Sunlight (Xe Lamp)	2.26	0.56	-	Biomass Valorization; Benzyl Alcohol to Benzaldehyde (Rate: 6.75 mmol m^{-2} h^{-1}).

The micro-patterned Optofluidic Microreactor (OFMR) developed in this work, utilizing a Pt–CdS photocatalyst under visible LED irradiation, demonstrates a scalable reactor architecture with an area-normalized hydrogen evolution rate (R_{area}) of 12.48 mmol m^{-2} h^{-1} and a mass-normalized rate (R_{mass}) of 1.21 mmol g^{-1} h^{-1}, achieving an Apparent Quantum Yield (AQY) of 0.11%. When benchmarked against (i) Microfluidic Reactors, the OFMR's performance is competitive with recent glass-based systems, such as the serpentine OFMRs reported by Rambabu et al., which achieved rates of 26.5 mmol m^{-2} h^{-1} and up to ~60.7 mmol m^{-2} h^{-1} with advanced corrugation and heterojunctions, while offering distinct fabrication advantages over micro-pillared or micro-grooved PDMS architectures that focus on flow perturbation. In the category of (ii) Scalable Rigid/Fixed Panel Reactors, the OFMR's active bubble removal and continuous flow operation contrast with passive systems like the 100 m^2 $SrTiO_3$:Al array by Nishiyama et al. (STH 0.76%, ~103 mmol m^{-2} h^{-1}) and the 1 m^2 panel by Goto et al. (STH 0.4%, ~28 mmol m^{-2} h^{-1}), though it does not yet match the high-intensity performance of concentrated sunlight systems (STH 6.2%). Finally, compared to (iii) Scalable Flexible Membrane Panel Reactors, the OFMR aligns with emerging PVDF-based immobilized systems. While Li et al. reported significantly higher rates (213.48 mmol m^{-2} h^{-1}, STH 0.68%), the OFMR's rate is comparable to piezo-photocatalytic membranes (15.71 mmol m^{-2} h^{-1}, STH 0.06%) and biomass-valorizing hybrid films (2.26 mmol m^{-2} h^{-1}), highlighting its potential for durable and stable hydrogen production.

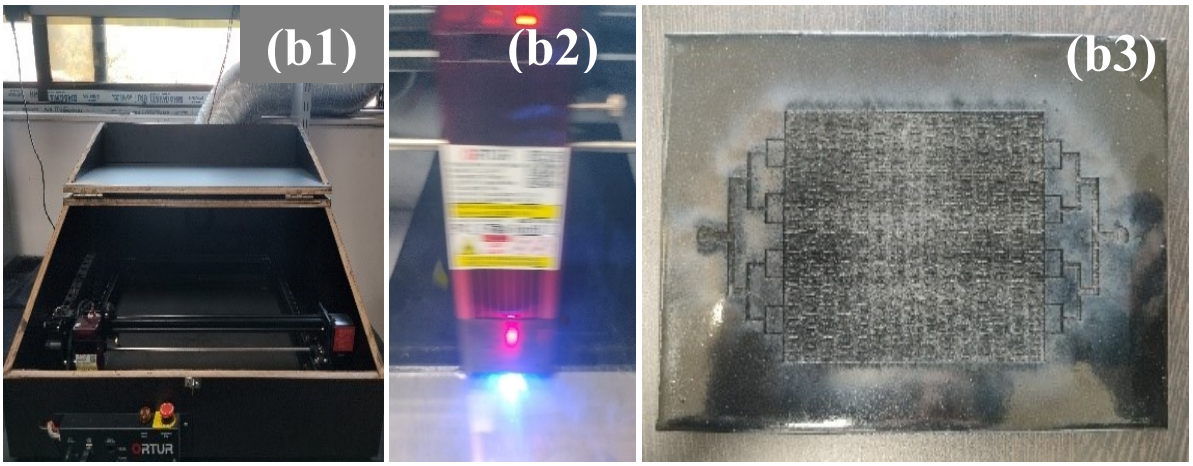
(b1)
(b2)
(b3)

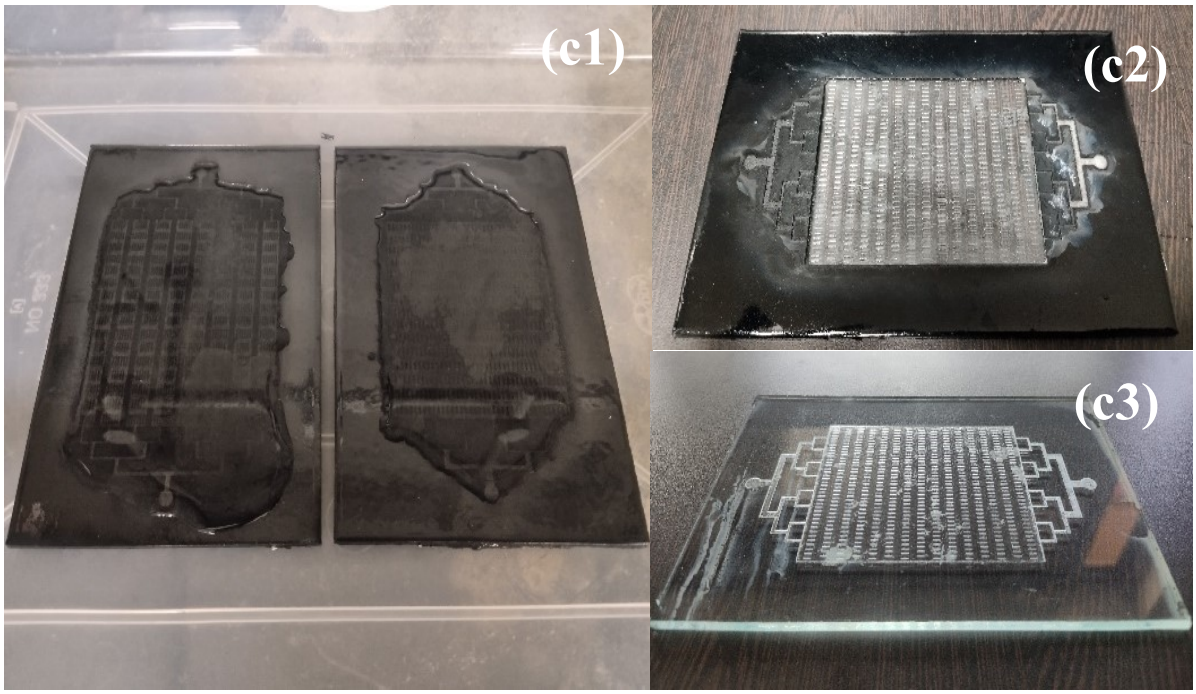
(c1)
(c2)
(c3)


(d1)
(d2)

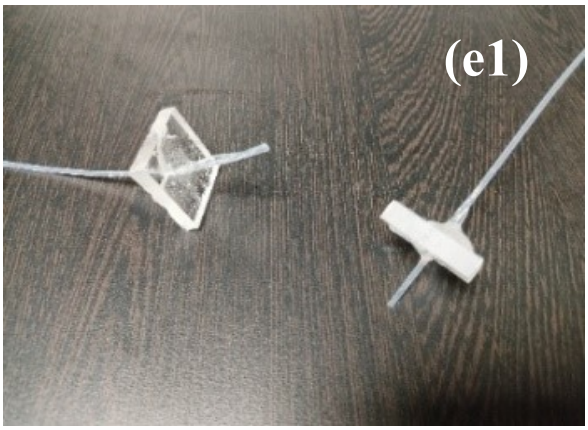
(e1)

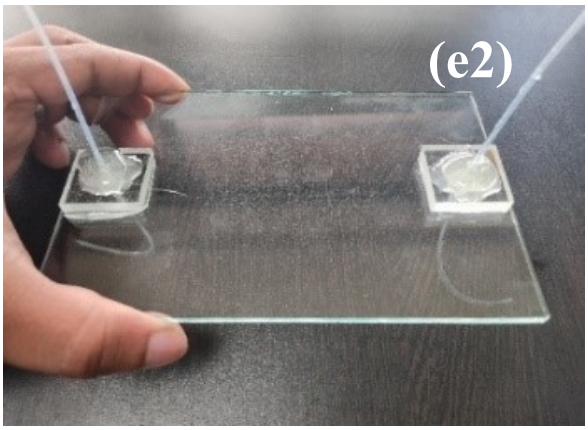
(e2)


UV-GLUE
(e3)

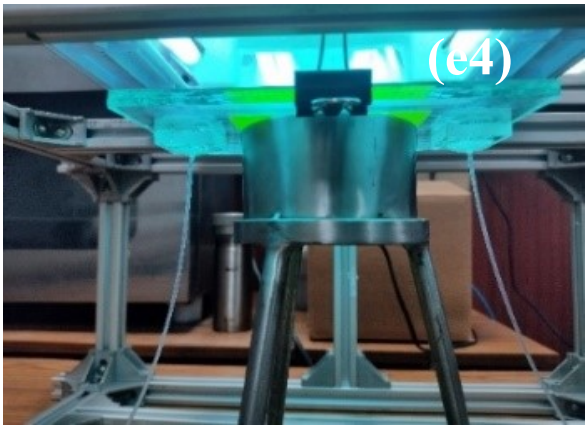
(e4)

Figure S1: Epoxy coating setup consisting of a paint gun and a painting platform (a1) and epoxy coated 152 mm x 102 mm glass sheets (a2 & a3); Laser engraver/cutting tool (b1 &b2) and the laser machined epoxy-coated glass sheet (b3); HF etching bath (c1) and microreactor plate after etching process (c2 & c3); Spray coating of photocatalysts onto reactor plates: airbrush used for spray coating (d1), spray coating process (d2), and spray coated reactor plates (d3 & d4); Steps involved in reactor construction: Inlet/outlet tubing with acrylic support (e1), top reactor window with glued inlet outlet connections (e2), reactor plates before sandwiching (e3), and UV glue curing of sandwiched reactor plates(e4).

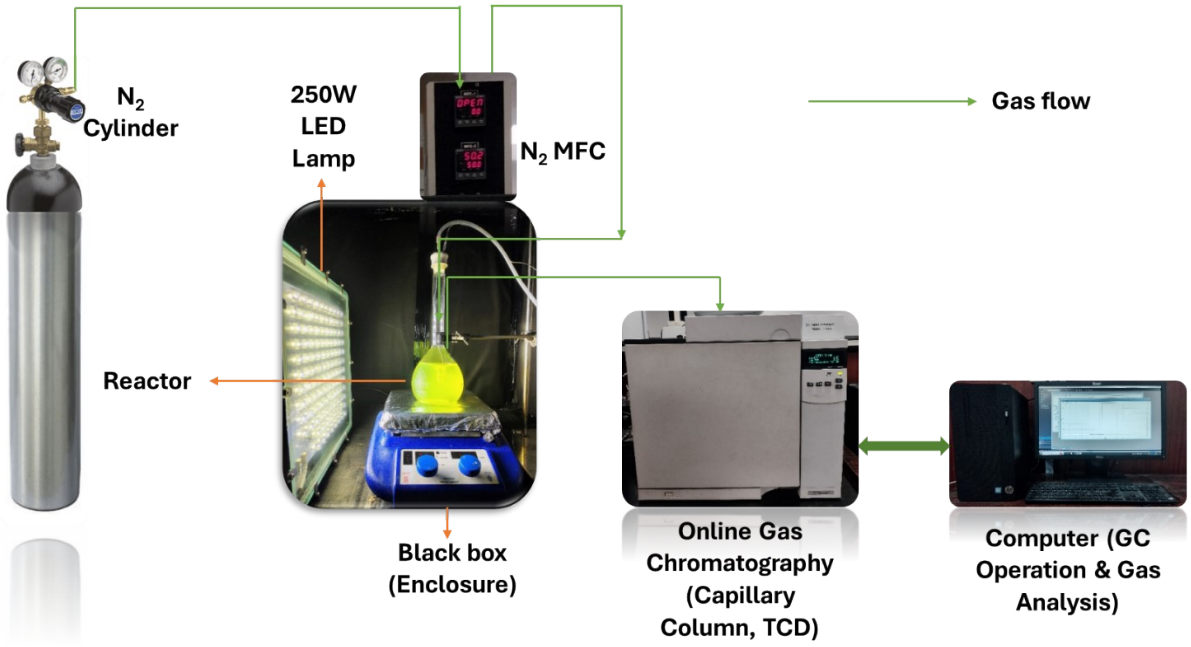

Figure S2: Photocatalytic hydrogen production experimental setup with particle suspension reactor

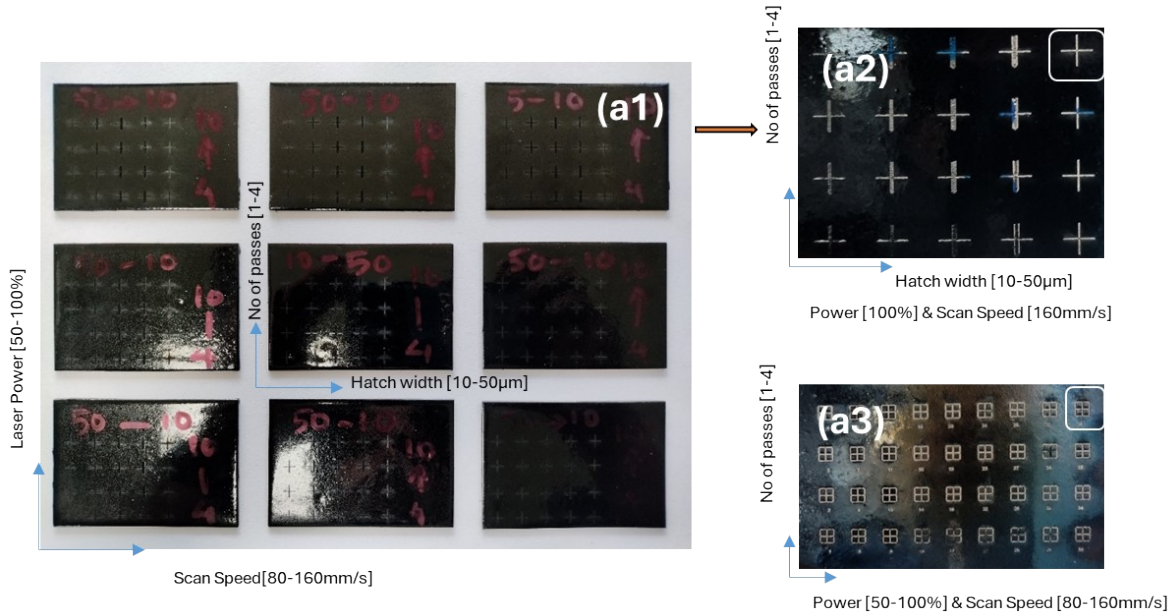

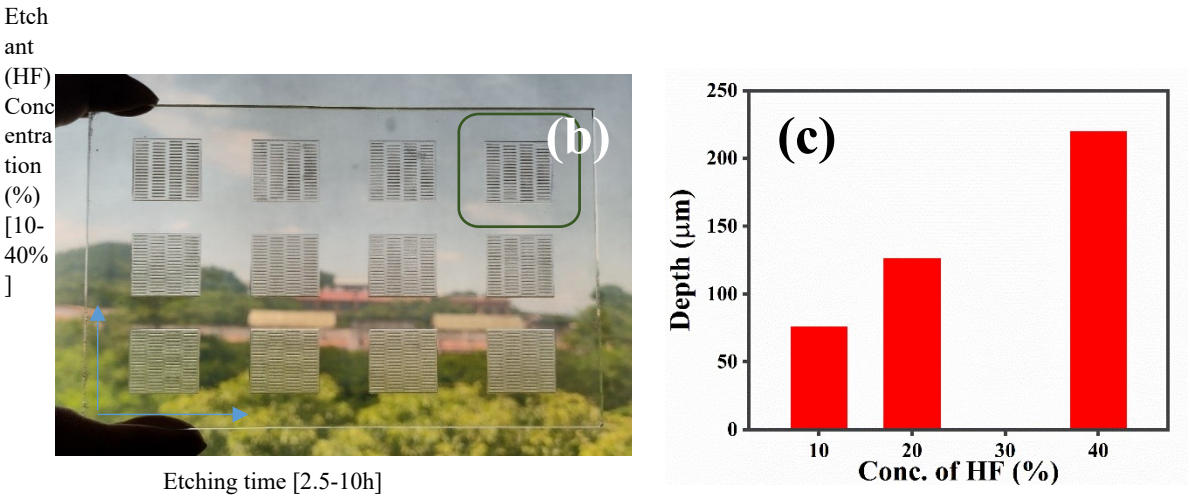

Figure S3: Minimalistic patterns made for optimization of laser machining parameters for machining of epoxy coated glass sheets (a1-a3), minimalistic patterns made for optimization of wet chemical etching parameters for the etching of laser machined epoxy coated glass sheets (b), and the graph showing variation of etch depth vs HF concentration for an etching duration of 10h (c).

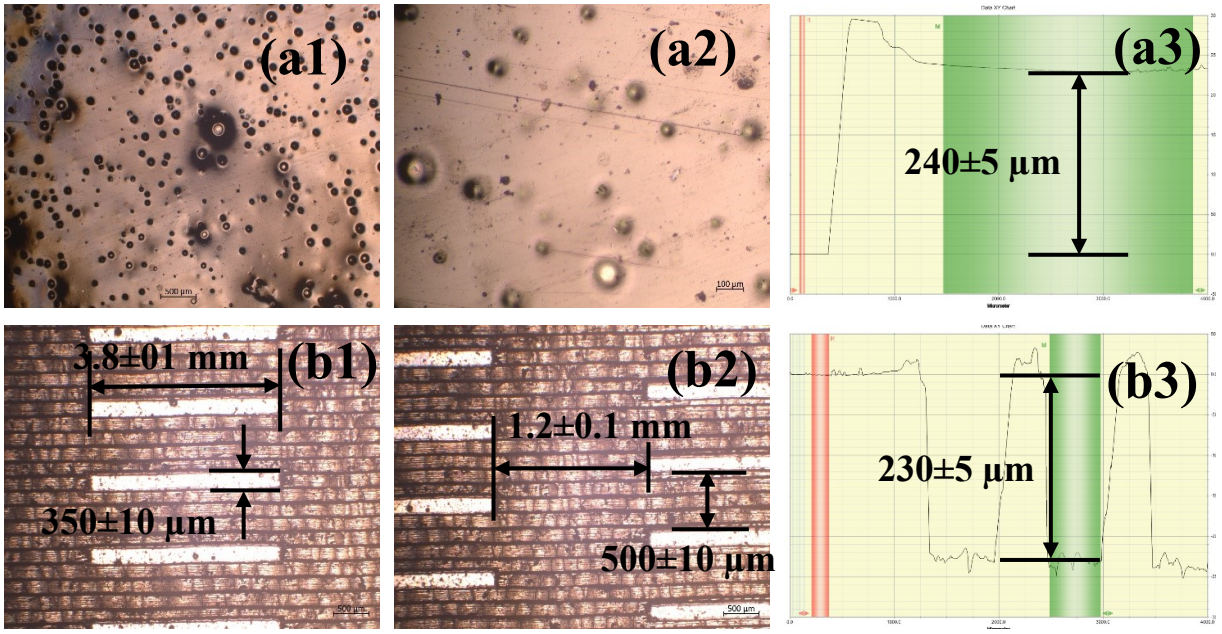

Figure S4: Characterization of the first two reactor plate fabrication steps. Optical microscopy images and a surface profilometry depth scan of an epoxy-coated glass sheet (a1-a3); optical microscopy images and a surface profilometry depth scan of a laser machined epoxy coating (100% power, 160 mm/s scan speed, 10 µm scan width, and 4 number of passes) (b1-b3).

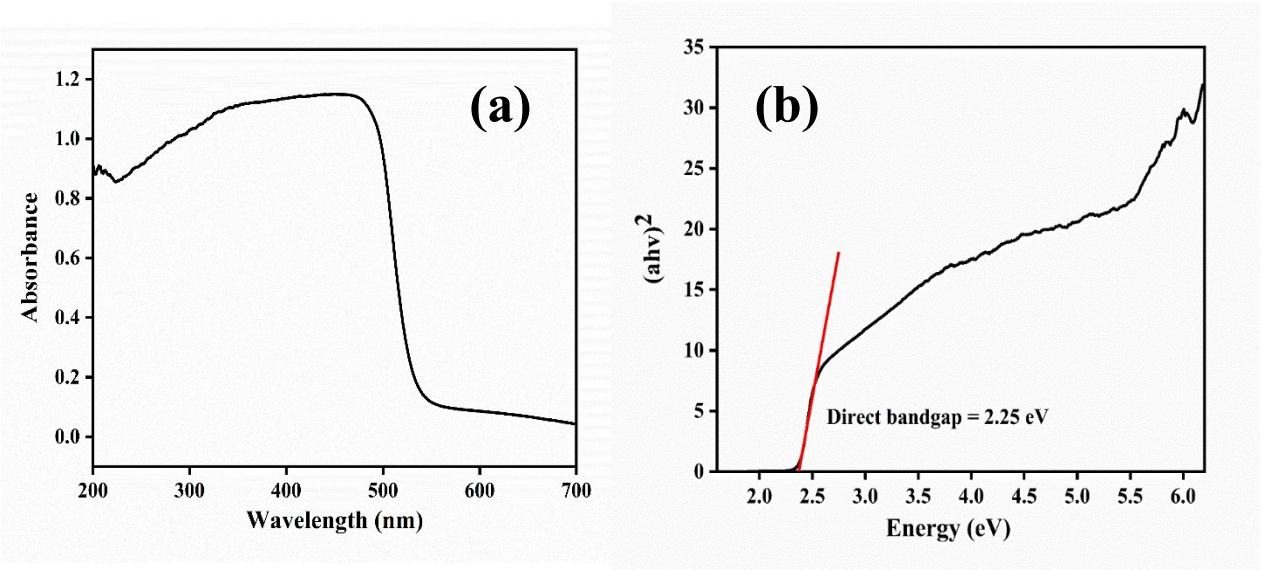
(a)
Absorbance
Wavelength (nm)
(b)
(ahv)2
Energy (eV)
Direct bandgap = 2.25 eV

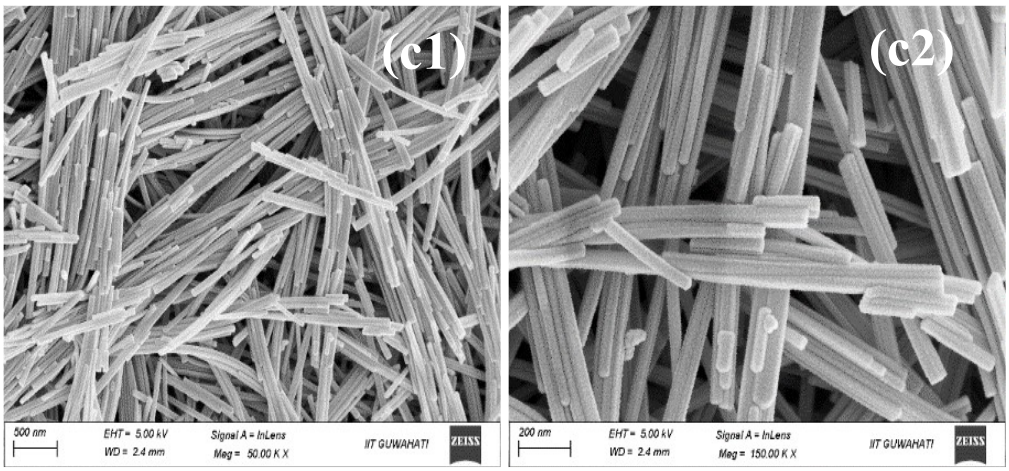
(c1)
(c2)
IIT GUWAHATI
ZEISS

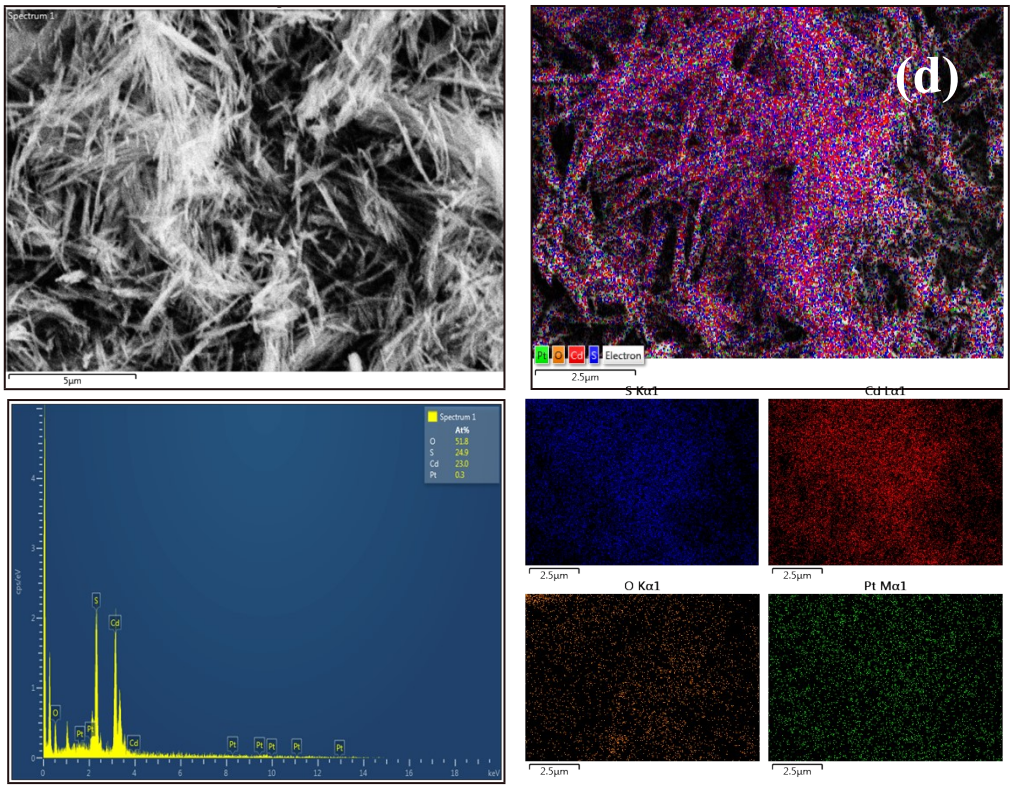
(d)
Electron
S Kα1
Cd Lα1
O Kα1
Pt Mα1

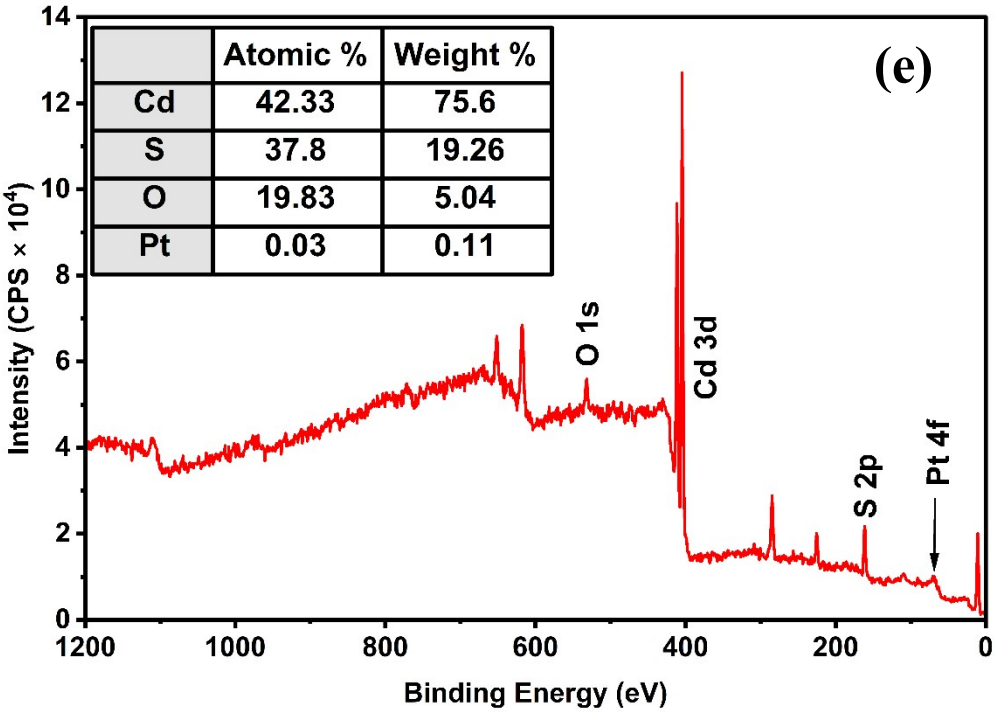

Figure S5: Characterization of the photocatalyst material. (a) UV-Visible absorption spectra of bare CdS nanowires; (b) Tauc plot derived from the UV-Vis absorbance spectra of CdS nanowires; (c1-c2) Scanning electron microscopy images of bare CdS nanowires; (d) EDX elemental mapping and composition spectra of Pt loaded CdS nanowires; and (e) XPS survey spectrum of the Pt-CdS photocatalyst. The inset table provides the quantitative elemental composition (excluding adventitious carbon), confirming a Pt cocatalyst loading of ~0.11 wt.%.

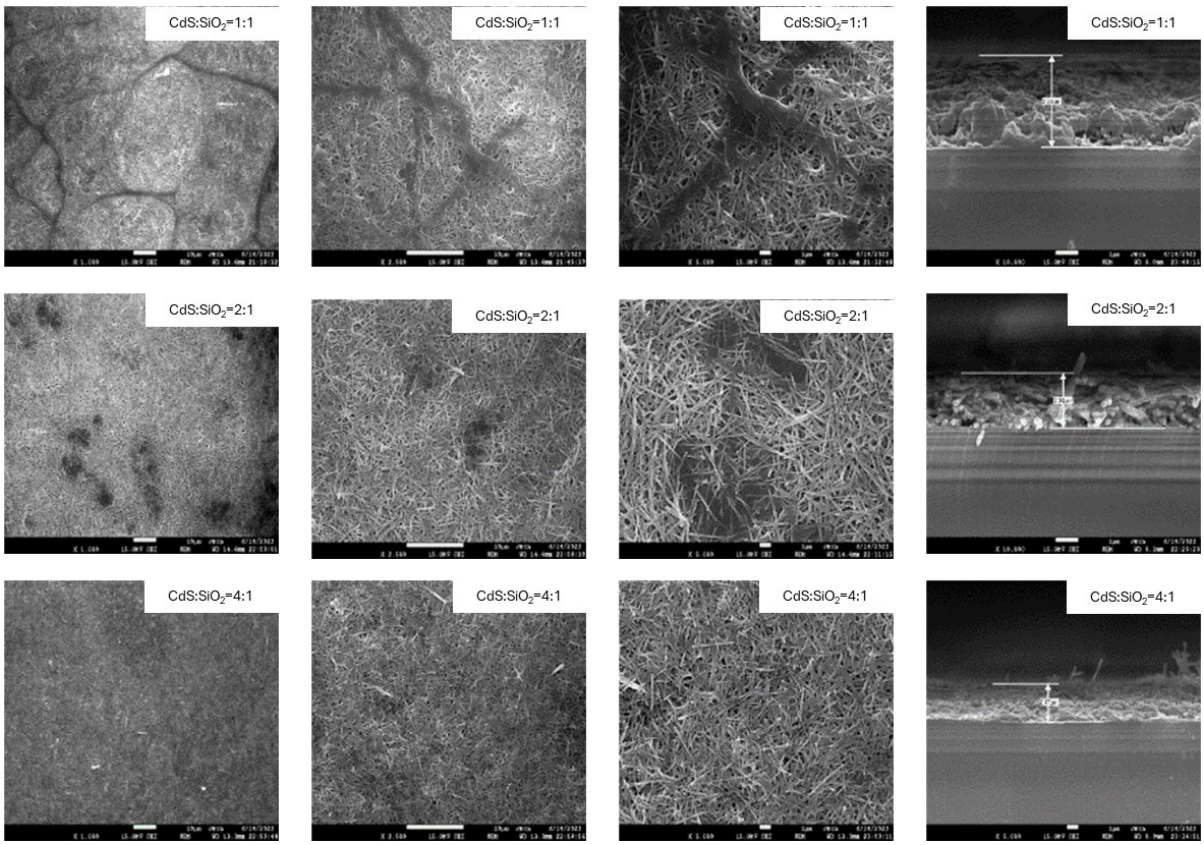
CdS:SiO2=1:1
CdS:SiO2=1:1
CdS:SiO2=1:1
CdS:SiO2=1:1
CdS:SiO2=2:1
CdS:SiO2=2:1
CdS:SiO2=2:1
CdS:SiO2=2:1
CdS:SiO2=4:1
CdS:SiO2=4:1
CdS:SiO2=4:1
CdS:SiO2=4:1

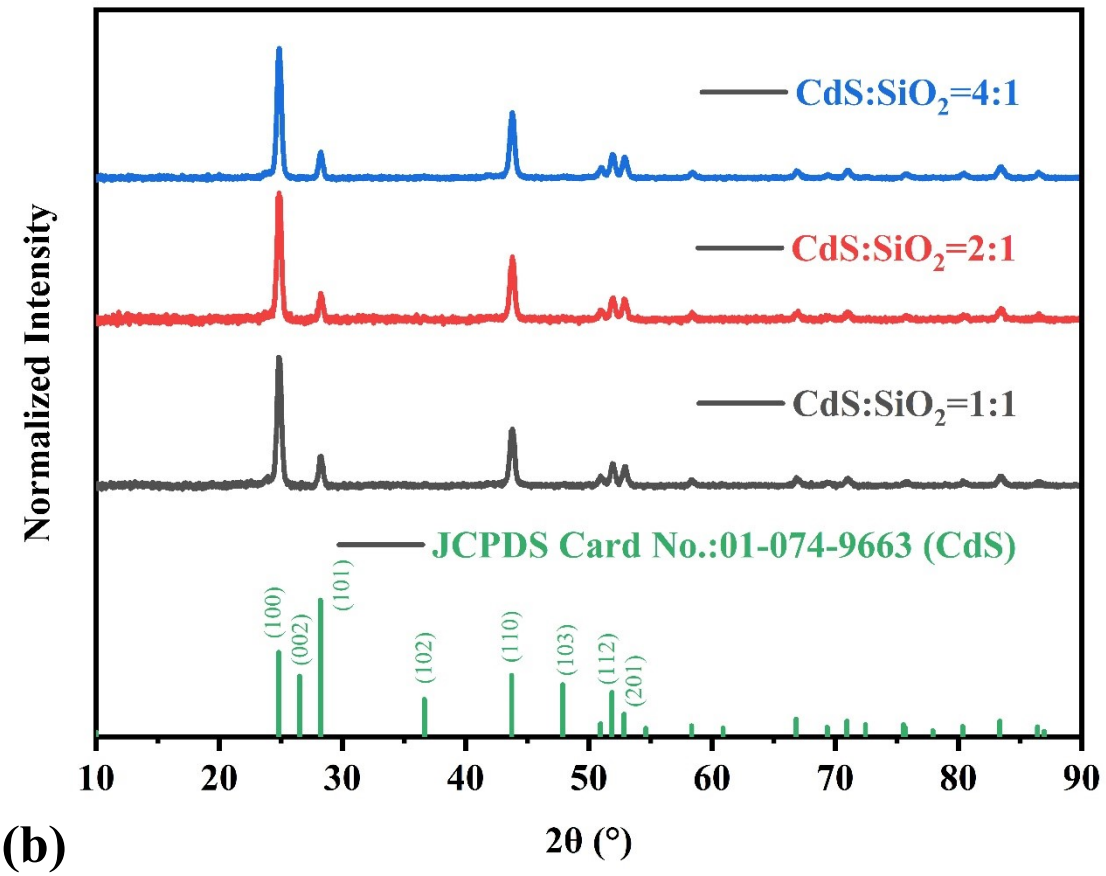
CdS:SiO2=4:1
CdS:SiO2=2:1
CdS:SiO2=1:1
JCPDS Card No.:01-074-9663 (CdS)
(100)
(002)
(101)
(102)
(110)
(103)
(112)
(201)
Normalized Intensity
10
20
30
40
50
60
70
80
90
2θ (°)

(b)

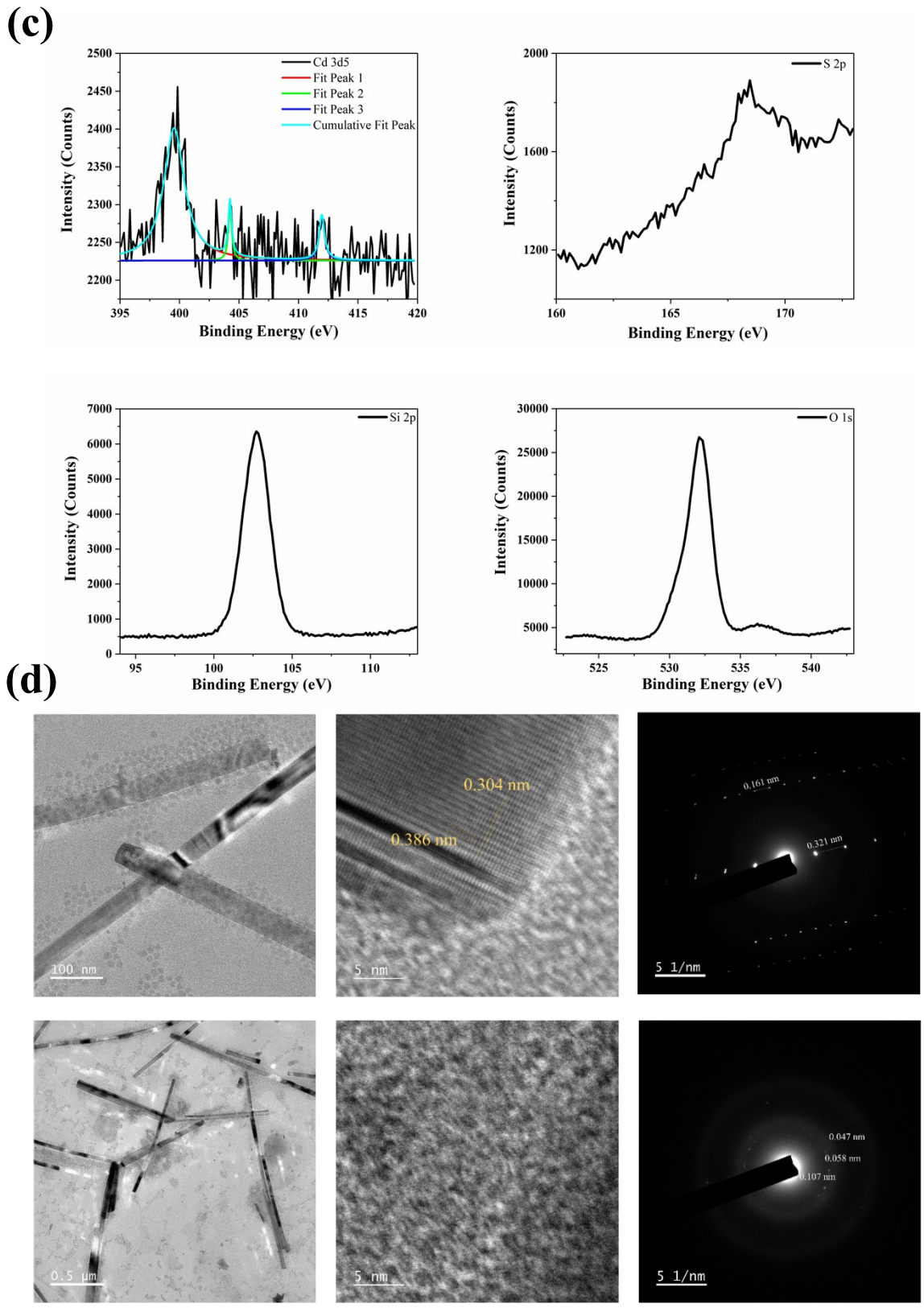

Figure S6: Characterization of the photocatalyst coatings. SEM images of catalyst coatings with various CdS:SiO_2 ratios (a), XRD spectra of catalyst coating samples with various

$CdS:SiO_2$ ratios (b), TEM images, HRTEM images, and SAED patterns of Pt-$CdS:SiO_2$ (1:1) mixture (c), and XPS spectra of Pt-$CdS:SiO_2$ (1:1) photocatalyst coating (d).

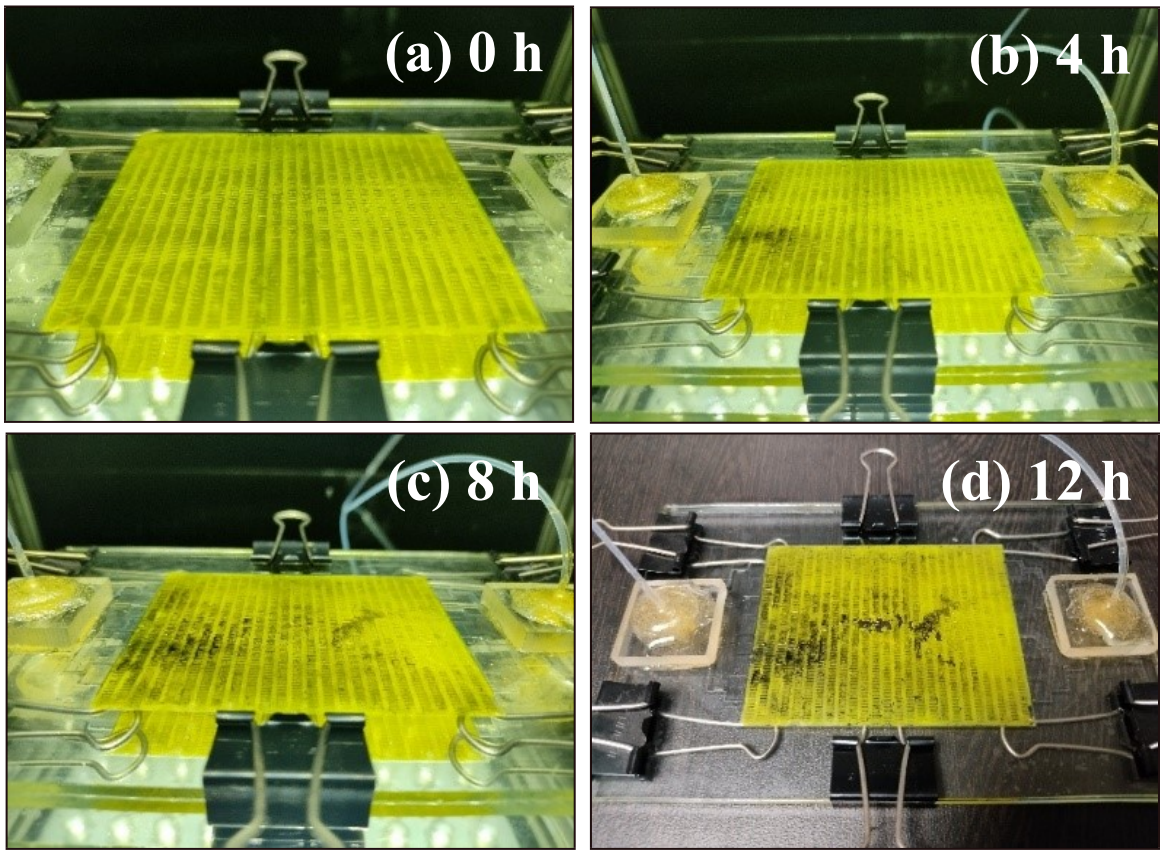

Figure S7: Visual documentation of catalyst layer durability during the 12-hour continuous flow experiment. Photographs of the optofluidic microreactor surface taken at (a) 0 h, (b) 4 h, (c) 8 h, and (d) 12 h. The images display a progressive reduction in coating coverage and exposure of the glass substrate, which becomes most pronounced between 4 and 12 hours. This physical degradation correlates directly with the plateau in catalytic activity observed in Figure 9, confirming that performance loss is driven by the synergistic effects of mechanical leaching (due to fluid shear stress) and the intrinsic photocorrosion of the CdS nanowires.

References:

(1) Fabian, D. M.; Hu, S.; Singh, N.; Houle, F. A.; Hisatomi, T.; Domen, K.; Osterloh, F. E.; Ardo, S. Particle Suspension Reactors and Materials for Solar-Driven Water Splitting. *Energy and Environmental Science*. Royal Society of Chemistry October 1, 2015, pp 2825–2850. https://doi.org/10.1039/c5ee01434d.

(2) Jing, D.; Guo, L.; Zhao, L.; Zhang, X.; Liu, H.; Li, M.; Shen, S.; Liu, G.; Hu, X.; Zhang, X.; Zhang, K.; Ma, L.; Guo, P. Efficient Solar Hydrogen Production by Photocatalytic Water Splitting: From Fundamental Study to Pilot Demonstration. *Int J Hydrogen Energy* 2010, *35* (13), 7087–7097. https://doi.org/10.1016/j.ijhydene.2010.01.030.

(3) Goto, Y.; Hisatomi, T.; Wang, Q.; Higashi, T.; Ishikiriyama, K.; Maeda, T.; Sakata, Y.; Okunaka, S.; Tokudome, H.; Katayama, M.; Akiyama, S.; Nishiyama, H.; Inoue, Y.; Takewaki, T.; Setoyama, T.; Minegishi, T.; Takata, T.; Yamada, T.; Domen, K. A Particulate Photocatalyst Water-Splitting Panel for Large-Scale Solar Hydrogen Generation. *Joule* 2018, *2* (3), 509–520. https://doi.org/10.1016/j.joule.2017.12.009.

(4) Nishiyama, H.; Yamada, T.; Nakabayashi, M.; Maehara, Y.; Yamaguchi, M.; Kuromiya, Y.; Nagatsuma, Y.; Tokudome, H.; Akiyama, S.; Watanabe, T.; Narushima, R.; Okunaka, S.; Shibata, N.; Takata, T.; Hisatomi, T.; Domen, K. Photocatalytic Solar Hydrogen Production from Water on a 100-M2 Scale. *Nature* 2021, *598* (7880), 304–307. https://doi.org/10.1038/s41586-021-03907-3.

(5) Chen, R.; Li, L.; Zhu, X.; Wang, H.; Liao, Q.; Zhang, M. X. Highly-Durable Optofluidic Microreactor for Photocatalytic Water Splitting. *Energy* 2015, *83*, 797–804. https://doi.org/10.1016/j.energy.2015.02.097.

(6) Li, L.; Chen, R.; Liao, Q.; Zhu, X.; Wang, G.; Wang, D. High Surface Area Optofluidic Microreactor for Redox Mediated Photocatalytic Water Splitting. *Int J Hydrogen Energy* 2014, *39* (33), 19270–19276. https://doi.org/10.1016/j.ijhydene.2014.05.098.

(7) Rambabu, P.; Peela, N. R. In-Situ CdS Nanowires on g-C3N4 Nanosheet Heterojunction Construction in 3D-Optofluidic Microreactor for the Photocatalytic Green Hydrogen Production. *Int J Hydrogen Energy* 2023, *48* (41), 15406–15420. https://doi.org/10.1016/j.ijhydene.2023.01.041.

(8) Rambabu, P.; Patel, S.; Gogoi, D.; Uppaluri, R. V. S.; Peela, N. R. Optofluidic Microreactor for the Photocatalytic Water Splitting to Produce Green Hydrogen. *Int J Hydrogen Energy* 2022, *47* (4), 2152–2163. https://doi.org/10.1016/j.ijhydene.2021.10.171.

(9) Zhou, P.; Navid, I. A.; Ma, Y.; Xiao, Y.; Wang, P.; Ye, Z.; Zhou, B.; Sun, K.; Mi, Z. Solar-to-Hydrogen Efficiency of More than 9% in Photocatalytic Water Splitting. *Nature* 2023, *613* (7942), 66–70. https://doi.org/10.1038/s41586-022-05399-1.

(10) Schröder, M.; Kailasam, K.; Borgmeyer, J.; Neumann, M.; Thomas, A.; Schomäcker, R.; Schwarze, M. Hydrogen Evolution Reaction in a Large-Scale Reactor Using a Carbon Nitride Photocatalyst under Natural Sunlight Irradiation. *Energy Technology* 2015, *3* (10), 1014–1017. https://doi.org/10.1002/ente.201500142.

(11) Li, W.; Duan, W.; Liao, G.; Gao, F.; Wang, Y.; Cui, R.; Zhao, J.; Wang, C. 0.68% of Solar-to-Hydrogen Efficiency and High Photostability of Organic-Inorganic Membrane Catalyst. *Nat Commun* 2024, *15* (1). https://doi.org/10.1038/s41467-024-51183-2.

(12) Ma, T.; Liao, G.; Gao, F.; Duan, W.; Wang, Y.; Cui, R.; Wang, C.; Li, W. Flexible Hybrid Membrane with Synergistic Exciton Dynamics for Excessive 280 h of Durably Piezo-Photocatalytic H2O-to-H2 Conversion. *Small* 2024, *20* (52). https://doi.org/10.1002/smll.202408056.
(13) Cui, R.; Li, W.; Duan, W.; Wang, Y.; Gao, Q.; Huang, Y.; Tuo, X.; Li, R.; Ma, W. Platinum Co-Catalysis Modulation of Exciton Dynamics and Film Loading for Durably Photoactive Benzyl Alcohol Value-Added Conversion and Hydrogen Co-Production. *Appl Catal B* 2025, *378*. https://doi.org/10.1016/j.apcatb.2025.125571.